Chapter 10

Fiber-Based High-Power Supercontinuum and Frequency Comb Generation

Qiang Hao, Tingting Liu and Heping Zeng

Additional information is available at the end of the chapter

http://dx.doi.org/10.5772/64209

Abstract

Ultrafast optics has been a rich research field, and picosecond/femtosecond pulsed laser sources seek many applications in both the areas of fundamental research and industrial life. Much attention has been attached to fiber lasers in recent decades as they offering various superiorities over their solid-state counterparts with compact size, low cost, and great stability due to the inherent stability and safety of the waveguide structures as well as high photoelectric conversion efficiency. Fiber-based sources of ultrashort and high-peak/high-average optical pulses have become extremely important for high-precision laser processing while sources whose carrier-envelop offset and repetition rate are stabilized can serve as laser combs with applications covering many research areas, such as precision spectroscopy, optical clock, and optical frequency metrology. For the application as laser combs, four parts as fiber laser, broadband supercontinuum, nonlinear power amplification, and repetition rate stabilization must be concerned. This chapter is intended to give a brief introduction about the achievement of the four technologies mentioned above with different experimental setups, recently developed such as divided-pulse amplification (DPA) in emphasize. Moreover, detailed descriptions of the experimental constructions as well as theoretical analyses about the phenomena they produced are also involved.

Keywords: fiber lasers, divided-pulse nonlinear amplification, four-wave mixing, frequency stabilized

1. Introduction

Ultrafast laser sources and their applications such as high-power supercontinuum and frequency comb have gained much attention in recent decades [1–7]. High-power fiber lasers

spur a rapid growth of industrial applications including laser cutting, laser marking, and so on [8]. Moreover, supercontinuum and frequency comb are considered as the breakthrough of laser field for their applications covering precision spectroscopy, astronomical observations, and optical frequency metrology [9, 10]. This chapter is intended to describe, from experimental point of view, the ultrashort pulse laser oscillators, high-power nonlinear fiber amplifiers, supercontinuum, and frequency combs. Section 2 shows the performance of two types of mode-locked lasers. The first one consisting of bulk and fiber optical components is mode-locked via nonlinear polarization rotation (NPR) mechanism at 1.03 μm. The other one, operating at 1.55 μm, is mode-locked by nonlinear amplified loop mirror (NALM) with polarization-maintaining (PM) fiber components in order to overcome environmental perturbation and thus maintain long-term operation. Section 3 introduces a practical method (spectral tailoring), which facilitates supercontinuum generation in single-mode fiber amplifier at 1.03 μm with a few picosecond laser pulses. The second part in this section introduced broadband supercontinuum generation (from 950 to 2200 nm) by injecting pulses with 72-fs temporal duration, 150-mW average power, and 60-MHz repetition rate at 1560 nm into 20-cm-long PM-HNLF. Section 4 gives a brief introduction of divided-pulse amplification (DPA). To generate transform-limited pulse at 1.55 μm, DPA with polarized pulse duplicating was employed to overcome the gain narrowing effect and control the nonlinear spectral broadening in anomalous dispersion Er-fiber amplifier. As high as 500-mW average power at 1560 nm is achieved by ×8 replicas. Moreover, the highest frequency-doubling conversion efficiency reached 56.3% by using a periodically poled lithium niobate (PPLN) crystal at room temperature. Section 5 discusses an all-optical control method via resonantly enhanced optical nonlinearity (or pump-induced refractive index change, RIC) for high-precision repetition rate stabilization. The standard deviation (SD) of repetition rate can be reduced to a record level of <100 μHz by using the RIC method in a PM figure-eight laser cavity.

2. Fiber laser

Fiber lasers offer several practical advantages, such as excellent spatial-mode quality, effective heat dissipation, and flexible optical path and, recently, are becoming attractive laser sources in both scientific researches and industry applications. Especially, mode-locked fiber lasers with ultrashort pulse duration and high-repetition rate have attracted a lot of attention for their applications in optical sensing, optical communication, optical metrology, and biomedical imaging and processing [11, 12]. Therefore, various femtosecond/picosecond mode-locked lasers have been constructed and developed. As mode-locked lasers are often affected by environmental perturbations (mechanical vibration and temperature fluctuation), robust and stable oscillator with compact design are urgently needed. In this section, we present a compact femtosecond fiber laser at 1.03 μm by using integrated fiber optical components. The shortest dechirped pulse duration reaches 81 fs for a net cavity dispersion value close to −0.001 ps^2. Another part of this section described a self-started Er-doped laser oscillator, which is mode-

http://dx.doi.org/10.5772/64209

locked by NALM with PM-fiber configuration. By optimizing the net dispersion, the build-up time can be reduced from 8 min to ~ms order of magnitude.

2.1. Operation regime of mode-locked lasers

As well known, the main features of mode-locked fiber laser depend on the pulse evolution process, which is relevant to the group-velocity dispersion (GVD) and the nonlinearity in optical fibers. According to the net intra-cavity dispersion, the pulse-shaping process can be roughly distinguished into the four different regimes, such as soliton regime, stretch-pulse regime, parabolic-pulse regime, and giant-chirp pulse regime, corresponding to all-anomalous dispersion, normal-anomalous dispersion, all-normal dispersion, and large-normal dispersion, respectively. Due to the equilibrium between Kerr nonlinearity and GVD, pulses that propagate in all-anomalous dispersion laser cavity keep unchanged in the form of fundamental soliton [13, 14]. While in dispersion-managed laser cavities, the negative dispersion is compensated by positive dispersion and thus stretch pulse forms. When the net cavity dispersion is optimized to zero, significant variations on pulse duration could be observed [15, 16]. As pulse operates in the all-normal dispersion regime, where laser gain, self-phase modulation, and dispersion co-effect, spectral/temporal filtering effects force linear chirping in the pulse, so that similariton forms [17–19]. While in ultra-long laser cavity, giant-chirped oscillating can be realized with ultralow repetition rate but at high-pulse energy [20–23].

2.2. NPR mode locking at 1.03 μm

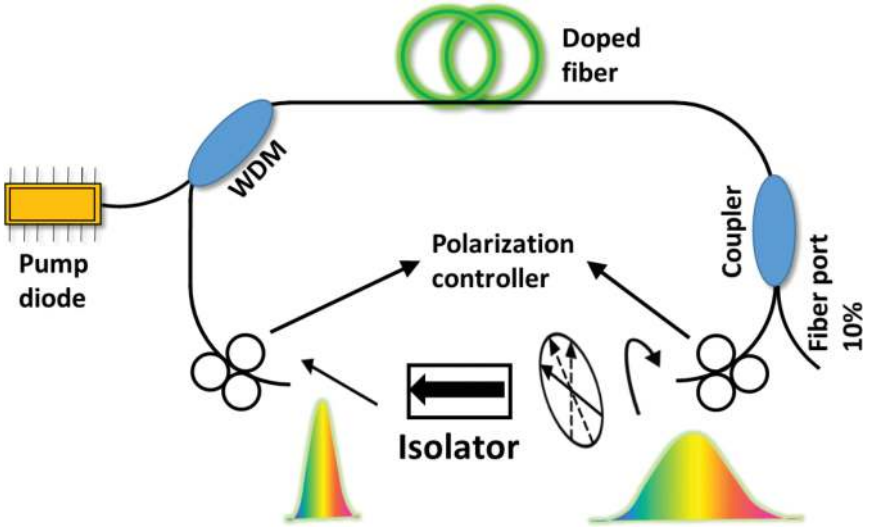

Figure 1. Schematic diagram of a passively mode-locked fiber laser via nonlinear polarization rotation mechanism.

In this section, we designed a compact ultra-fast Yb-doped fiber laser with integrated optical components. By integrating wavelength division multiplexer and optical isolator with collimators, the fiber loop was simplified. Self-started mode-locking could be realized by setting appropriate polarization angle of four intra-cavity wave plates. Due to the normal dispersion of fiber at 1.0 μm, transmission grating pair with 1250 l/mm was used to provide adjustable anomalous dispersion. As a result, 81-fs temporal duration with 65-MHz repetition rate and 0.5-nJ pulse energy was produced.

The mode-locking procedure can be explained in **Figure 1**. Two polarization controllers and a polarization-sensitive isolator (PSI) are used as the key elements for mode-locking. This combination acts as a virtual saturable absorber, which can absorb the low-intensity tail of pulse and transmit high-intensity part such that the pulse could be shortened. The pulse with linear polarization changes to elliptical polarization by twisting the polarization controller. As mentioned, self-phase modulation (SPM) or cross-phase modulation (XPM) can arouse energy coupling between two orthogonal polarizations. Moreover, serious nonlinear polarization rotation is produced by the high gain in the active fiber. Finally, another polarization controller is used to modify the polarization state to facilitate the central part of the pulse getting through the PSI [24].

In our experiment, a Yb-doped fiber laser shown in **Figure 2(a)** was firstly constructed without dispersion compensation elements. Three intra-cavity wave plates including two quarter-wave plates, QWP1 and QWP2, and one half-wave plate, HWP, were set with appropriate polarization angles to realize self-started mode-locking. The pigtails of fiber components are Hi1060 fiber with GVD of ~26 fs^2/mm and TOD of ~41 fs^3/mm, while the GVD for the active fiber is 39 fs^2/mm. The repetition rate and pulse duration were measured to be 70 MHz and 13 ps, respectively. By external-cavity dechirping, the pulse can be compressed to 170-fs duration, but with obvious pedestal. The autocorrelation of pulse before and after dechirping is shown in **Figure 3(a)** and **(b)**, respectively.

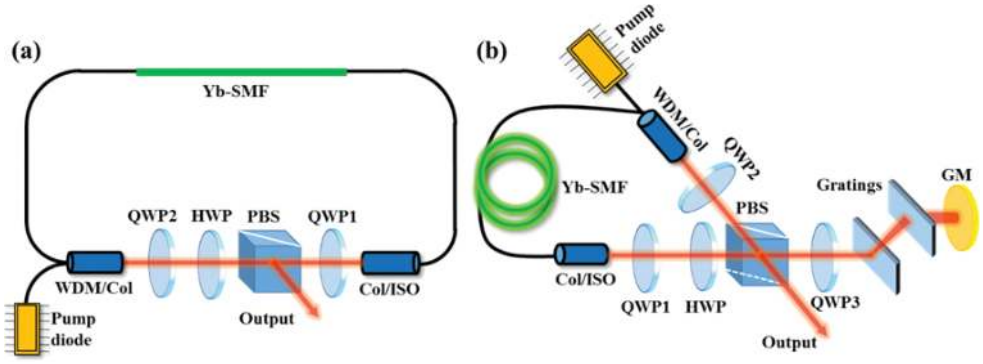

Figure 2. Structure of ultrafast Yb-doped fiber lasers without (a) and with (b) dispersion compensation. Pump diode: 400-mW laser diode at 976 nm; Yb-SMF: Yb-doped single-mode fiber; WDM/Col: the device combines WDM and colli-

mator; Col/ISO: the device combines collimator and isolator; QWP1, QWP2, and QWP3: quarter-wave plate; HWP: half-wave plate; PBS: polarization beam splitter; GM: a gold-coated mirror.

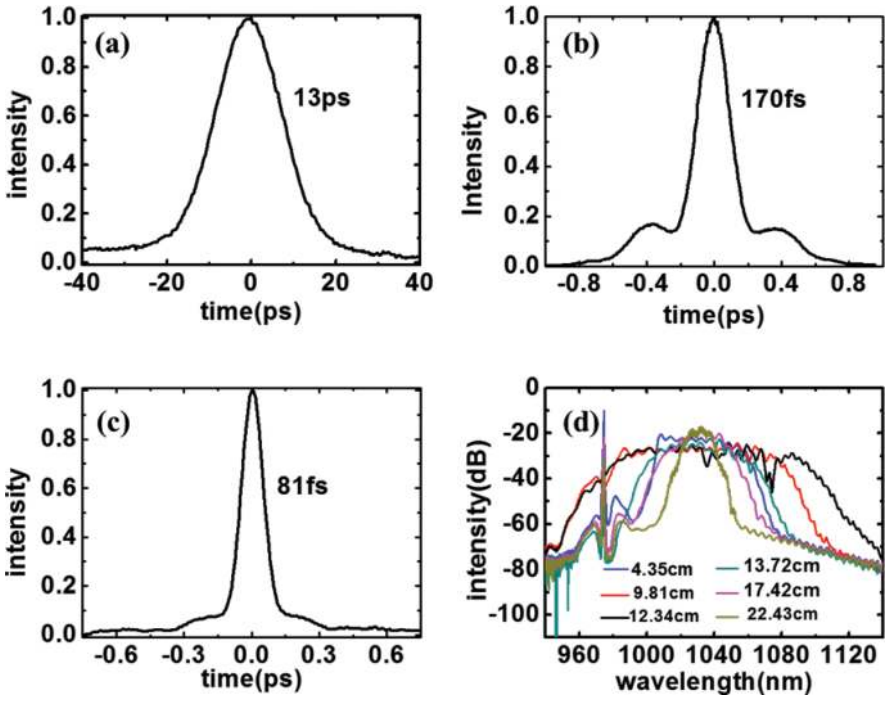

Figure 3. Autocorrelation trace of chirped pulses generated by picosecond fiber laser (a) and femtosecond fiber laser (c), (b) dechirped pulse of (a); (d) spectra generated by femtosecond fiber laser with different distances between gratings.

Secondly, a transmission grating pairs was used to manage the intra-cavity dispersion of the Yb-fiber laser, as shown in **Figure 2(b)**. The quarter-wave plate, QWP3, was used to impose 90° polarization rotation on laser pulses by double-passing the grating pairs. Soliton, stretch-pulse, and all-normal dispersion regime can be achieved by optimizing the distance between gratings. **Figure 3(d)** compares the various spectral shapes with different grating separations. As shown in **Figure 3(c)**, the shortest pulse duration was measured to be 81 fs. The black curve in **Figure 3(d)** represents the broadest spectra with a 10-dB bandwidth of 100 nm. The uncompensated phase was mainly caused by the accumulated high-order dispersion in fibers as well as intra- and extra-cavity grating pairs.

2.3. Polarization-maintaining figure-eight fiber laser at 1.55 μm

Compact size, low cost, and free maintenance fiber laser at 1.55 μm are desirable in many applications, such as eye surgery, Terahertz generation, and precision spectroscopy [25–28]. The standard repetition rate of commercial available fiber laser is typically 80 MHz with an

optional design from 20 to 250 MHz. In order to combine both high pulse energy and high average power, a 10-MHz repetition rate is the best choice for applications. When the repetition rate is lower than 10 MHz, a pulse picker has to be used between the laser oscillator and the succeeding amplifier.

In this section, we introduce a PM figure-eight laser cavity which is the best option for oscillator operated at 10-MHz repetition rate. **Figure 4(a)** shows the experimental setup of the figure-eight laser cavity. The linear loop comprises of a 980/1550 nm wavelength division multiplexer, a segment of Er-doped fiber (PM-ESF-7/125, Nufern), an isolator, a 2-nm bandpass filter at 1550 nm, and an output coupler CP2 with a splitting ratio of 20:80. The active gain applied in the linear loop is to compensate the cavity loses and facilitate self-started mode-locking. The band-pass filter is used to block longer wavelength (Raman self-frequency shift) and reduce the temporal width of the pulse to be self-consistent. Pulses from the linear loop are coupled into NALM via CP1 with a splitting ratio of 45:55.

Over-pump with three LDs was applied to provide enough power for self-started mode-locking. Interestingly, the buildup time of mode-locking was found to be closely related to the net cavity dispersion. When the net dispersion was set to −0.115 ps^2, as long as 8-min build-up time was observed. After optimizing the net dispersion to about −0.062 ps^2, the time dramatically decreased to ~ms of magnitude.

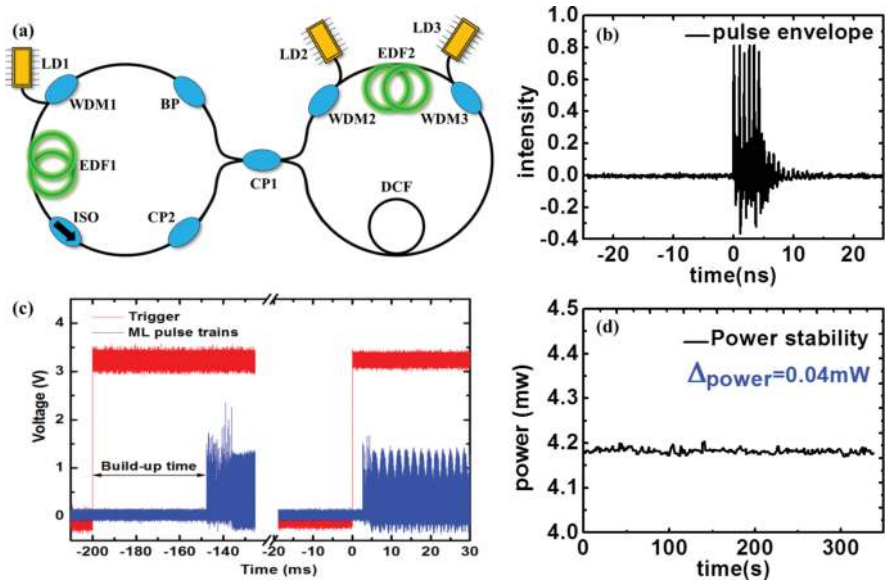

Figure 4. (a) Schematic of a polarization-maintaining figure-eight erbium-doped fiber laser. WDM1, WDM2, and WDM3: 980/1550 nm wavelength division multiplexers; ISO: isolator; EDF1 and EDF2: erbium-doped fiber; BP: 2-nm bandpass filter at 1550 nm; DCF: dispersion compensation fiber; CP1 and CP2: 1550 nm coupler with splitting ratio of 45:55 and 20:80. (b) The initial pulse that polarization-maintaining figure-eight erbium-doped fiber laser generated. (c) The buildup time measured by an oscilloscope. (d) The measurement of power stabilization once mode-locked.

Furthermore, we recorded the mode-locked pulse trains triggered by a square wave with 5-Hz modulation frequency which is simultaneously used to drive LD3. **Figure 4(c)** shows two adjacent periods with 50-ms pump duration, and the corresponding buildup time was measured to be 53 and 6 ms, respectively, exhibiting certain randomness. From experimental results point of view, the mode-locking buildup time is a random value in a certain range, which is related to the net cavity dispersion.

Interestingly, multiple-pulse operation was observed as the mode-locking is established, as shown in **Figure 4(b)**. Peak power clamping effect originating from sagnac mechanism resulted in the formation of pulse bunching [29]. Stable single pulse could be obtained by decreasing the pump power. In single-pulse regime, the 5-min power stability was measured to be 0.26%, as shown in the inset of **Figure 4(d)**.

3. Broadband supercontinuum

Recent years, supercontinuum generation (SC) has attracted much attention for its applications in optical coherence tomography, stimulated emission depletion microscopy, dense wavelength-division-multiplexing (DWDM) optical networks, and frequency comb generation [30–33]. In this section, several nonlinear optical effects such as SPM, XPM, four-wave mixing (FWM), and stimulated Roman scattering (SRS) that facilitate SC generation would be firstly discussed. Secondly, spectral filtering method is demonstrated to be an effective way for broadband supercontinuum generation in picosecond region [34]. By spectral filtering, a linear-chirped picosecond pulse with a 1-nm bandwidth filter installed between two Yb-doped single-mode preamplifiers, pulse shortening, and high peak power is achieved, so that an octave-spanning SC with bandwidth of 650 nm from 750 to 1400 nm and 10-dB peak-to-peak flatness was obtained at an output average power of 190 mW. Thirdly, SC covering from 950 to 2200 nm is generated in a 20-cm-long PM HNLF by injecting 72-fs pulse with 150-mW average power and 60-MHz repetition rate at 1.56 μm. Furthermore, an inline f-2f interferometer, including a PPLN for frequency doubling and a PM-fiber delay line, is used to generate carrier-envelop offset signal (f_{ceo}).

3.1. Nonlinear effects in optical fibers

Most of nonlinear effects in optical fibers attribute to nonlinear refraction, which refer to the intensity dependence of the refractive index. Especially, the lowest order nonlinear effects in optical fibers originate from the third-order susceptibility $\chi^{(3)}$, which governs the four-wave mixing, Raman effect, third-harmonic generation, and polarization properties [24].

This section does not thoroughly focus on the discussion of theoretical issues. In simple, the refractive index of the optical fiber can be described by the following equation

$$n = n_0 + n_1 \left| E(t) \right|^2 \tag{1}$$

where n_0 is the linear part and $n_1 |E(t)|^2$ is the nonlinear part.

An interesting phenomenon of the intensity dependence of the refractive index change in optical fiber occurs through SPM. When the input pulse is of low intensity, the corresponding refractive index remains a constant n_0. As the input pulse increases, the corresponding refractive index becomes nonlinear change with power intensity I. Hence, an additional phase shift is produced:

$$\delta\varphi(\mathrm{t}) \propto \left|E(t)\right|^2 \tag{2}$$

This can be understood as an instantaneous optical frequency change from its central frequency:

$$\delta\omega(\mathrm{t}) = -\frac{\partial}{\partial \mathrm{t}}\delta\varphi(\mathrm{t}) \tag{3}$$

Therefore, new spectral components are generated and time dependent frequency chirping is produced.

Another most widely studied nonlinear effect is XPM, which leads to asymmetric spectral and temporal changes for two co-propagating optical fields with different wavelength or orthogonally polarization. The contribution of the nonlinear phase shift induced by XPM is twice that of SPM. Therefore, the nonlinear part Δn_{j} induced by the third-order nonlinear effects is given by (j = 1, 2)

$$\Delta n_j \approx n_2\left(\left|E_j\right|^2 + 2\left|E_{3-j}\right|^2\right) \tag{4}$$

Eq. (4) shows the refractive index of the optical media seen by an optical field inside a single-mode fiber depends not only on the intensity of that field but also on the intensity of the other co-propagating fields [35]. As the optical field propagates inside the fiber, an intensity-dependent nonlinear phase shift shows up

$$\phi_j^{NL}(z) = n_2\left(\omega_j / c\right)\left(\left|E_j\right|^2 + 2\left|E_{3-j}\right|^2\right)z \tag{5}$$

The first term is related to SPM while the second term is related to XPM.

Stimulated Raman scattering (SRS) is an important nonlinear process that can produce red-shifted spectral components. Once the spectrum of the input pulse is broad enough, the Raman gain can amplify the long-wavelength components of the pulse with the short-wavelength components acting as pumps, and the energy appears red-shifted. The longer the propagat-

ing fiber, the more red-shifted spectral components can be generated. The red-shifted components are called Stokes wave. The initial growth of the Stokes wave can be described by

$$\frac{dI_s}{dz} = g_R I_p I_s \tag{6}$$

where I_s is the Stokes wave intensity, I_p is the pump-wave intensity, and g_R is the Raman-gain coefficient, which is related to the cross section of spontaneous Raman scattering.

The Raman-gain coefficient g_R (Ω) is the most important factor to describe SRS. Ω represents the frequency difference between the pump wave ω_p and Stokes wave ω_s. In the case of silica fibers, the Raman-gain spectrum is found to be very broad, extending up to approximately 40 THz. Assuming the pump wavelength is 1.5 μm and, peak gain is $g_R = 6 \times 10^{-14}$ m/W, the frequency downshift can be calculated to be 13.2 THz.

When supercontinuum is generating in an optical fiber, the SPM, XPM, and SRS are always accompanied by FWM. In optical fibers, FWM transfers energy from pump wave (ω_p) to two other waves in frequency domain, blue-shifted (anti-Stokes wave, ω_{as}) and red-shifted (Stokes wave, ω_s). Once the phase-matching condition $\Delta k = 2k(\omega_p) - k(\omega_s) - k(\omega_{as}) = 0$ is satisfied, the Stokes and anti-Stokes waves can be amplified from noise or an incident signal at ω_s or ω_{as}, respectively [36, 37]. Therefore, FWM process is used to produce spectral sidebands for supercontinuum generation.

3.2. Supercontinuum generation

SC is a powerful laser sources for many applications, such as nonlinear microscopy, optical coherence tomography, and frequency metrology [38–40]. Nowadays, more than one octave SC can be easily generated with a length of PCF, and the average power can reach tens of Watts [41, 42]. When ultrashort optical pulses propagate through a PCF fiber, the combination of SPM, XPM, SRS, and FWM is responsible for the spectral broadening. Generally speaking, the feature of SC depends on whether the incident laser wavelength λ located is below, closed to, or above the Zero-dispersion wavelength λ_D of the PCF. In the anomalous-dispersion regime ($\lambda > \lambda_D$) where $\beta_2 < 0$, soliton affects. If the λ nearly coincides with λ_D, $\beta_2 \approx 0$, β_3 dominant and the phase-matching condition of FWM are approximately satisfied. While in the normal-dispersion regime, $\beta_2 > 0$, GVD and SPM effects dominant SC generation. From the time domain of view, SPM and soliton effects dominant SC generation for femtosecond (typically <1 ps) pump pulses, while FWM and SRS contribute to spectral broadening for tens of picoseconds pulses.

3.2.1. Spectrally filtered seed for broadband supercontinuum generation in single-mode fiber amplifiers

There are several methods to extend the SC spectrum. Considerable spectral broadening could be observed with high-power incident laser. High-average/high-peak powers facilitate CW and pulse SC generation [43–45]. Besides, the SC bandwidth could also be increased by tapering PCFs. A flat (3 dB) spectrum from 395 to 850 nm was achieved in a tapered fiber with

a continuously decreasing ZDW [46]. In this section, we demonstrate an effective method for broadband SC generation, which is valid in normal-dispersion fiber amplifiers. By spectral filtering of upchirped pulse at 1028 nm with 1-nm bandpass filter, as broad as 650-nm bandwidth from 750 to 1400 nm within 10-dB peak-to-peak flatness is obtained with an output power of 190 mW.

The experimental setup is shown in **Figure 5(a)**. The SC laser source is consisted of a picosecond mode-locked laser oscillator, a spectral filter, two-stage single-mode amplifiers, and 2-m-long PCF with ZDW at 1.02 μm. The laser oscillator operated in an all-normal-dispersion regime with repetition rate of 20 MHz. With 100 mW pumping power, 25 mW average output power laser is exported from the 30% port of the coupler. The pulse duration of highly upchirped pulse was measured to be 10 ps.

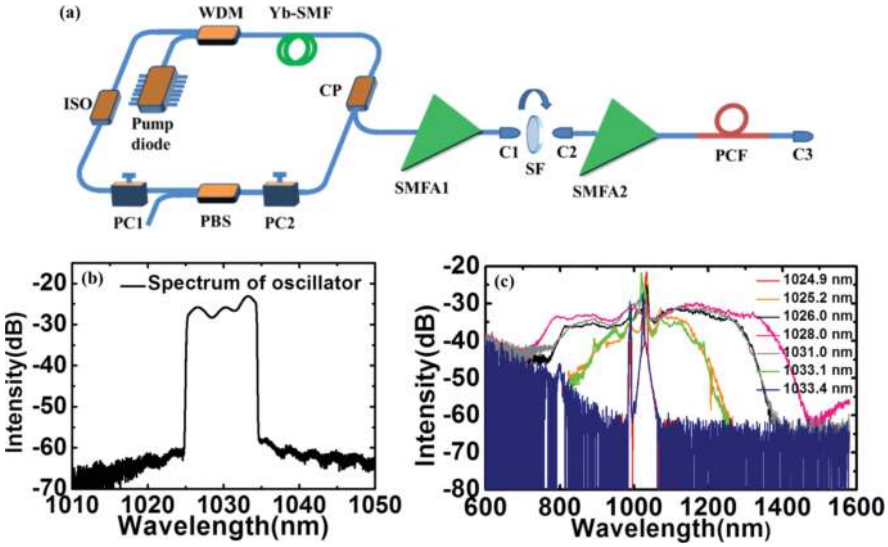

Figure 5. (a) Experimental setup for SC generation. Pump diode: 400 mW laser diode at 976 nm; WDM: 980/1040 nm wavelength division multiplexer; Yb-SMF: ytterbium-doped single-mode fiber; CP: 30:70 coupler; PC1 and PC2: polarization controller; PBS: polarization beam splitter; ISO: isolator; SMFA1 and SMFA2: single-mode fiber amplifiers; C1, C2, and C3: three collimators; SF: spectral filter; PCF: photonics crystal fiber. (b) The output spectrum of the laser oscillator. (c) SC with different filtering windows.

A bandpass spectral filter with 1-nm bandwidth at 1036 nm is installed between two single-mode fiber amplifiers. The transparent wavelength of the filter could be tuned from 1024 to 1036 nm by varying the incident deflection angle. For the large up-chirp with 10-nm spectral width (see **Figure 5(b)**) and 10-ps temporal duration, corresponding to a time-bandwidth product of 28.3, pulse can be greatly shortened by the filter. The shortest pulse duration of 2.9 ps was obtained with filtering window at 1028 nm. After the second-stage amplifier, the laser pulses could be amplified to an average power up to 190 mW with 400 mW pumping power.

http://dx.doi.org/10.5772/64209

A 2-m length of silica-based PCF with ZDW at 1024 nm is directly spliced to the fiber end of SMFA2. **Figure 5(c)** shows the output spectrum with different filtering window. The spectra keep unchanged when the filtering window is at the shoulder of the spectrum, shown as the red curve (1024.9 nm) and blue curve (1033.4 nm) in **Figure 5(c)**. When filtering window is located at the central wavelength of 1028 nm, the 10-dB bandwidth of SC is extended to 650 nm (from 750 to 1400 nm), shown as the pink curve in **Figure 5(c)**. Besides, filtering windows above or below the central wavelength produce a less broad SC.

3.2.2. One octave supercontinuum for frequency comb generation

Broadband supercontinuum of bandwidth up to 1250 nm can also be provided by HNLFs with spectral-tailored femtosecond pump pulses produced by erbium-doped power amplifiers. The schematic diagram of the experiment is shown in **Figure 6(a)**.

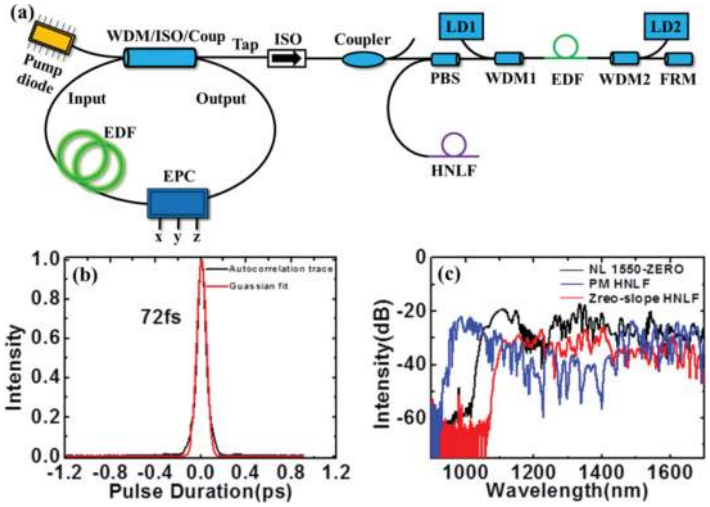

Figure 6. (a) Schematic diagram for SC generation. Pump diode: 400-mW pump at 976 nm; WDM/ISO/Coup: the device combines wavelength division multiplexer, isolator, and coupler; EDF: erbium-doped fiber; EPC: electric polarization controller; ISO: isolator; coupler: 30:70 polarization-maintaining coupler; PBS: polarization beam splitter; HNLF: high nonlinear fiber; LD1 and LD2: pumps at 976 nm; WDM1 and WDM2: 980/1550 nm wavelength division multiplexer; FRM: Faraday rotation mirror. (b) Autocorrelation trace of chirped pulses poured into HNLFs. (c) SC generated by different kinds of HNLFs on logarithmic coordinate.

The laser system consisted of an erbium-doped mode-locking fiber oscillator, a single-mode fiber amplifier (SMFA), and 20-cm-long PM-HNLF. To improve the mode-locking stability, an electric polarization controller (EPC) is utilized to replace the conventional mechanical polarization controller such that automatic and active control of mode-locking is accessible. By applying the voltage on three axes (x, y, and z) of EPC, accurate control of the temporal duration, spectral shape, f_{rep}, and f_{ceo} can be achieved [47, 48].

With the help of a PBS and a FRM, a dual-pass single-mode fiber amplifier with bidirectional pump configuration was used to boost the laser average power to more than 150 mW average power and reduce the environmental disturbance on SMFA. The pulse duration at the output port was measured to be 2.84 ps. Additional PM-1550 fiber was used to dechirp the pre-amplified pulse to 72 fs (shown in **Figure 6(b)**). Therefore, considering a repetition rate of 60 MHz, the pulse peak power achieved as high as 34.7 kW. Three types of HNLFs, such as NL 1550-ZERO, PM-HNLF, and Zero-slope HNLF, were applied to generate the supercontinuum by splicing the HNLFs to the dechirping fiber directly.

As shown in **Figure 6(c)**, 20-cm-long PM-HNLF with nonlinearity of 10.5 W^{-1} km^{-1} achieved the broadest spectrum, covering from 950 to 2200 nm, which is sufficient broad to produce f_{ceo} signal. The HNLF type should be taken into consideration as it influences the SC generation. We used three kinds of HNLFs: 25-cm-long NL 1550-ZERO with nonlinear coefficient of 10.4-W^{-1} km^{-1} and effective mode area of 13-μm^2, 20-cm-long PM-HNLF with nonlinear coefficient of 10.5-W^{-1} km^{-1} and effective mode area of 12.7-μm^2, 25-cm-long Zero-slope HNLF with nonlinear coefficient of 10.8-W^{-1} km^{-1} and effective mode area of 12.4-μm^2, and the corresponding SC was depicted in **Figure 6(c)**. Obviously, PM-HNLF produces broader spectrum than other two HNLFs.

As shown in **Figure 7**, a collinear setup was established for the detection of f_{ceo} signal. The SC generated by 20-cm-long PM-HNLF was coupled into free space via a lens (L1) with adjustable focal length. An inline f-2f interferometer, including a PPLN, several wave plates and lens, and a PM-fiber delay line, is used to produce the temporal overlapped components at 1.0 μm. The long-wavelength component of SC at 2092 nm was frequency doubled to match with the short-wavelength component at 1046 nm. After the PPLN, two lenses, L3 and L4, were used to couple the two components at 1046 nm back to PM-980 fiber. A half-wave plate, HWP2, is used to adjust the energy ratio on the fast and slow axes of PM-980 fiber. The pulse transmitted along the slow axis experiences a delay relative to the pulse on fast axis. With an optimized fiber length of 3.4 m, the differential delay between the fast and slow axes could be fully

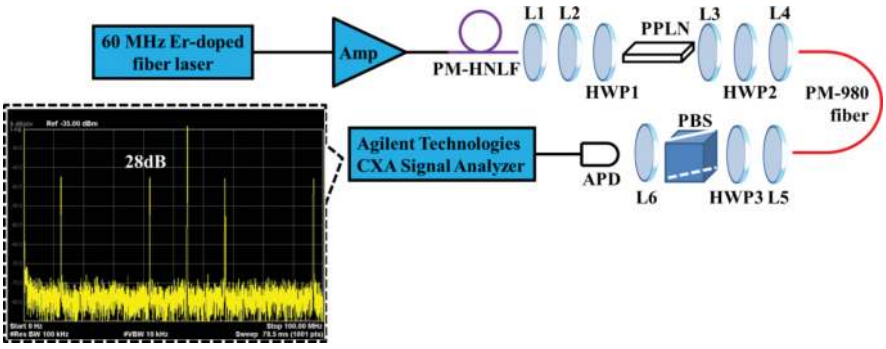

Figure 7. Setup for f_{ceo} detection. Amp: fiber amplifier; L1, L4, and L5: optical lens with adjustable focal length; L2, L3, and L6: optical lens with focal length of 50 mm; HWP1, HWP2, and HWP3: half-wave plates; PPLN: periodically poled lithium niobate; PBS: polarization beam splitter; APD: avalanche photodiode.

http://dx.doi.org/10.5772/64209

compensated [49]. Subsequently, a half-wave plate, HWP3, as well as a PBS were used to selected pulses to generate f_{ceo} signal on APD. Finally, with 28-dB signal-to-noise ratio was generated by using this setup.

4. Nonlinear fiber amplifier

With the increasing applications in frequency metrology, THz generation, and in cataract surgery, the development for high-energy transform-limited pulse generation around 1.55 μm is still a fascinating area [50–53]. Owing to the limited available output power from laser oscillator, erbium-doped fiber amplifiers (EDFAs) are commonly used. Nevertheless, high-power amplification in EDFA is inevitably accompanied by several unwanted effects, such as SRS and amplified spontaneous emission (ASE), which would significantly deteriorate the temporal and spectral duration of pulse [54]. Chirped-pulse amplification (CPA) provides an effective way to decrease pulse peak power and avoid the nonlinearity in optical fibers [55–58]. In CPA, strong stretching and compression occurs to extract more energy and avoid nonlinear distortion as well as damage. However, CPA is inevitably accompanied by the gain-narrowing effect and therefore hardly produces pulse with temporal duration less than 400 fs [59].

Even though CPA has many advantages over the other techniques in amplifying pulses around 1.55 μm, ~100-fs pulse duration with above 10-nJ pulse energy is still a challenge because of the spectral gain-narrowing effects and nonlinear phase accumulation. Moreover, due to the involvement of bulk media, CPA is not suited for applications that require compact size and alignment-free laser source. A recent developed technique, divided-pulse amplification (DPA), opens up a new way for high-power laser pulse amplification [60–62].

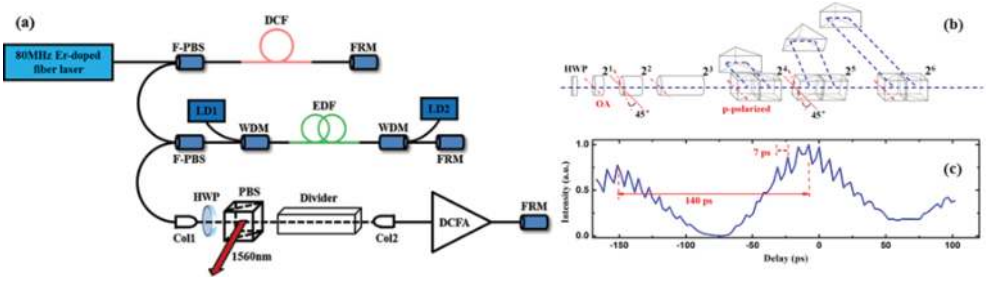

Figure 8. (a) Schematic diagram for laser system. F-PBS: fiber-coupled polarization beam splitter; DCF: dispersion compensation fiber; FRM: Faraday rotation mirror; LD1, LD2: pump diodes at 976 nm; WDM: wavelength division multiplexer; EDF: erbium-doped single-mode fiber; Col1, Col2: high-power collimators; HWP: half-wave plate; PBS: polarization beam splitter cube; DCFA: double-clad fiber amplifier. (b) Schematic of the pulse divider. The left-hand three cylinders (21, 22, and 23) represent YVO4-based dividers with given direction of crystal optical axes (OAs) shown as the red dash dot lines. The right-hand three parts (24, 25, and 26) represent PBS-based dividers with p-polarized direction shown as red dash dot lines. The red dot lines represent the horizontal plane, which is the same direction as the OA of 21 and 23 and the p-polarized direction of 24 and 26. (c) The measured autocorrelation trace of the divided replicas.

In the configuration of DPA, the initial pulse is divided into a sequence of lower-intensity pulse with orthogonal polarization for successive replicas, and subsequently, the low-energy pulse is amplified and then recombined to create a high-energy pulse [61, 63].

In this section, we mainly focus on DPA at 1.56 μm where pulse amplification and compression can be simultaneous carried out so that a separate compressor is no longer necessary. The schematic diagram of DPA is shown in **Figure 8(a)**. The experimental setup is composed of a mode-locked fiber laser, a fiber stretcher, a single-mode fiber amplifier for preamplifying, and a pulse-divider as well as a double-clad fiber amplifier for main amplification. The Er-doped fiber laser with 80-MHz repetition rate shared the same configuration as **Figure 6(a)**, which takes the advantage of EPC to actively control the mode-locking. A photodiode and an electric loop were applied to monitor and feedback control the EPC for long-term stable operation. The fiber oscillator consisted of 1.74-m SMF28-e fiber with dispersion parameter of 19 ps/nm/km and 0.82-m Er-doped fiber with dispersion parameter of −51 ps/nm/km. There, the laser operated in the stretched-pulse regime and produced positively chirped pulses. As a result, with 200-mW pumping power at 976 nm, the laser oscillator produces 5-mW output average power with 1.5-ps pulse duration and 28-nm spectral bandwidth, corresponding to a time-bandwidth product of 5.2.

A fiber stretcher is spliced to the output of the fiber oscillator to stretch laser pulse and control the quantity of frequency up-chirp. However, over-long fiber could inevitably introduce too much high-order dispersion which is hardly compensated by the pulse-compressing stage. For the current configuration, a double-pass fiber stretcher consisting of a fiber-coupled PBS with PM fiber at input/output port and non-PM fiber at common port, a segment of non-PM dispersion compensation fiber with 6.0-μm-mode field diameter and −38 ps/nm/km dispersion at 1550 nm, and a FRM is used to reduce the environmental perturbation.

In our experiment, 6-m dispersion compensation fiber was applied to stretch pulses from the fiber oscillator. A dual-pass bidirectionally pumped single-mode fiber preamplifier was used to boost the average power to more than 100 mW to ensure efficient operation of the subsequent amplifiers. A FRM reflected the incident pulse to suppress ASE noise and rotated the polarization of the pulses by 90° to cancel all birefringence effects in the dual-pass amplifier.

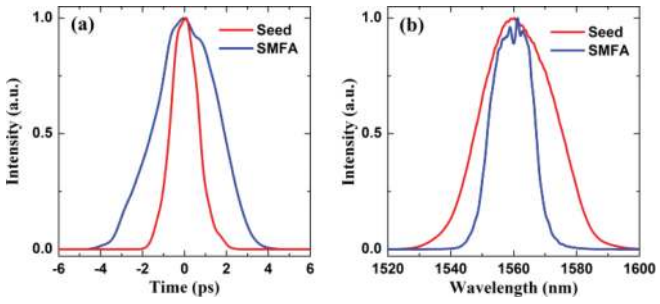

Figure 9. The temporal duration (a) and spectral bandwidth (b) of laser pulses from laser oscillator (red curves) and SMFA (blue curves).

http://dx.doi.org/10.5772/64209

A fiber-based polarization beam splitter (F-PBS) was used to couple the seed laser to the preamplifier and reflected preamplified pulses to subsequent components. The output characters of the preamplifier were shown as the blue curves in **Figure 9(a)** and **(b)**. The FWHM temporal duration and spectrum bandwidth of the preamplified pulses is 4 ps and 15 nm, respectively, generating a time-bandwidth product of 7.4. Dramatic decrease in spectral bandwidth was observed due to the limited transmission bandwidth of WDM and FRM as well as spectral-narrowing effect in fiber amplifier.

Then, the concept of DPA was carried out to boost the laser to Watt-level average power. The preamplified laser is coupled into free space by collimator C1 and rotated to horizontal polarization to reach maximum transmission on PBS. The pulse division and combination were achieved by applying cascaded YVO_4-based and PBS-based dividers with the help of a FRM to reflect the replicas passing through the same divider but in the opposite direction. Each divider (YVO_4-based or PBS-based) can divide a single pulse into two cross-polarized replicas; hence, a single seed pulse could be temporally divided into 2^N (where N is the stage number of the divider) replicas. Ideally, each replica has identical pulse energy after division. As depicted in **Figure 8(b)**, three YVO_4 crystals with lengths of 10, 20, and 40 mm divided the initial pulse into $N = 8$ replicas. A half-wave plate (HWP) was used to produce the desired polarization of input pulses. The first (2^1) and third (2^3) YVO_4 crystals had their crystal optical axes (OA) oriented in the same direction as the horizontal plane, while the OA of the second (2^2) YVO_4 crystal oriented at a 45° angle to the horizontal plane. The polarization-mode delay between ordinary and extraordinary waves in YVO_4 is 0.7 ps/mm at 1560 nm. The shortest crystal length for our system was chosen to split the input pulse into replicas with 7 ps separation, about twice of the seed pulse duration.

To mitigate the nonlinearity in main amplifier, the string of pulse ($N = 8$) was further divided by three PBS-based dividers, resulting in a final pulse number of 64. For PBS-based divider, each incoming pulse was divided into an s-polarized beam and a p-polarized beam. All p-polarized components were directly transmitted the PBS, while the s-polarized components were reflected to the folded delay line. For the sake of simplicity, the second PBS-based divider (2^5) had its p-polarized direction oriented 45° to the direction of the horizontal plane, while the first (2^4) and third (2^6) PBS-based oriented in the same direction as the horizontal plane, such that separate half-wave plates were no longer necessary.

Owing to the delay length of 10, 20, 40, 26.8, 53.6, and 107.2 mm, the 2^1, 2^2, 2^3, 2^4, 2^5, and 2^6 stages approximately provided time delay of 7, 14, 28, 130, 260, and 520 ps, respectively. **Figure 8(c)** shows the measured autocorrelation trace of the pulse string which matches well with the designed time delays. The 7-ps interval between adjacent peaks in the same envelope was consistent with the expected time delay with 10-mm increment length of YVO_4, and the ~140-ps spacing between two adjacent envelopes was consistent with the expected time delay introduced by the PBS-based divider.

Intuitively, for simultaneous pulse amplification and compression in EDFAs, a positively pre-chirping seed pulse is desired. Numerical simulations show that there exists an equilibrium position that can not only restrict excessive nonlinear effects to ensure high-quality temporal integrity but also produce sufficient optical nonlinearity to broaden the spectrum around the

wavelength of 1.55 μm. The generalized nonlinear Schrödinger equation (7) with the split-step Fourier method was used to carry out the simulation [24].

$$\frac{\partial A}{\partial z} = \frac{\alpha}{2} A + \sum\nolimits_{n\geq 2} \frac{i^{n+1}}{n!} \beta_n \frac{\partial^n A}{\partial T^n} + i\gamma A \int_{-\infty}^{\infty} R(T') \left| A(z, T - T') \right|^2 dT' \tag{7}$$

where $A = A(z, t)$ is the complex amplitude of the pulse envelope of pulses, α is the laser gain coefficient, β_n is the dispersion parameter at ω_0 (1560 nm), and γ (3 W^{-1} km^{-1}) is the nonlinear coefficient. The right-hand side of Eq. (7) models laser gain, dispersion, and nonlinearity. Pulse of 2.5-ps temporal duration and 19.9-nm spectral width (corresponding to 0.16 ps^2 prechirping on 180-fs transform-limited pulse) and a pulse energy of 0.05 nJ were applied in the simulation.

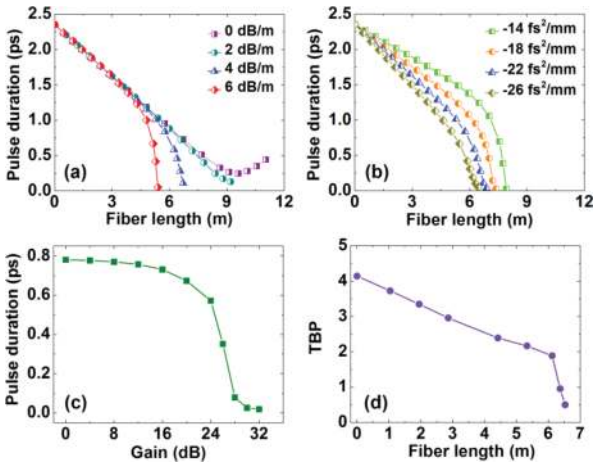

Figure 10. Amplified output pulse duration versus propagation length for the cases of different α (a) and β_2 (b). (c) Pulse duration versus the total gain provided by 6.5-m fiber. (d) Time-bandwidth product at different position of gain fiber.

The interplay of the SPM and group-velocity dispersion (GVD) as well as laser gain can lead to a qualitatively different behavior compared with that expected from them alone. SPM broadened the spectrum with increase in pulse energy, and simultaneously, the anomalous dispersion of the fiber compressed the new spectral components resulting in temporal shortening. **Figure 10(a)** compares the simulation results with different α but a fixed β_2 (−22 fs^2/mm). It is clear that pulse compression operates in linear regime when the laser gain is low, then it enters in nonlinear regime when the laser gain gradually increased. The shortest transform-limited pulse duration decreased from 180 fs at 7.0 m (α = 0 dB/m) to 60 fs at 4.3 m (α = 3 dB/m). **Figure 10(b)** compares the pulse compression with different β_2 but a fixed α

http://dx.doi.org/10.5772/64209

(3 dB/m). The maximum pulse energies with respect to fiber length of 4.65, 5.07, and 5.53 m reached 1.24, 1.66, and 2.28 nJ, respectively. Therefore, higher α and smaller $|\beta_2|$ are benefit to overcome spectral bandwidth limitation for high-energy pulse amplification. For reference, the blue curves in **Figure 10(a)** and **(b)** present pulse evolution with the same parameters.

Next, we focus on pulse amplification and compression in a fixed fiber length by way of guiding the subsequent experiment. About 5.0-m-long fiber with β_2 = −22 fs^2/mm was introduced to simulate the output pulse duration and the time-bandwidth product (TBP) at different position along the fiber. As shown in **Figure 10(c)**, when the total gain is smaller than 16 dB, the output pulse duration deceases linearly owing to the GVD and insufficient nonlinearity. As the total gain is greater than 24 dB, the output pulse duration dramatically decreases owing to strong nonlinear compression. Theoretically, pulse as short as 80-fs duration can be achieved with a total gain of nearly 28 dB. Although the pulse duration could be further decreased to 20 fs with 32-dB gain, considerable pedestal as well as wave breaking appears due to excessive nonlinearity. Meanwhile, the TBP of the pulse along the fiber gradually decreases from 4.1 at the input port to 0.5 at the output port.

Experimentally, the divider first operated with ×8 replicas. A dual-pass double-cladding fiber amplifier (DCFA) was used to boost the divided pulses. The DCFA consisted of 1.2-m 12/130 Er-doped double-clad fiber and 2.5-m SMF fiber. With a pump power of 4.3 W at 976 nm, the DCFA delivered 600 mW output power at 1560 nm, as measured at PBS output port. Along the first pass of DCFA, pulse evolution worked in the near-linear regime. Subsequently, as the pulse reflected by the FRM and passed through DCFA again, SPM and anomalous dispersion brought the pulse amplification into the moderate nonlinearity regime. **Figure 11(a)** and **(b)** shows pulse duration and spectral bandwidth of the combined pulse measured by an FROG (15-100-USB, Swamp Optics). The linear spectral phase indicates a nearly transform-limited pulse with the FWHM duration of 97 fs if a Gaussian pulse shape is assumed. The output power limitation was resulted from splicing losses of different type fibers and the insertion loss of FRM.

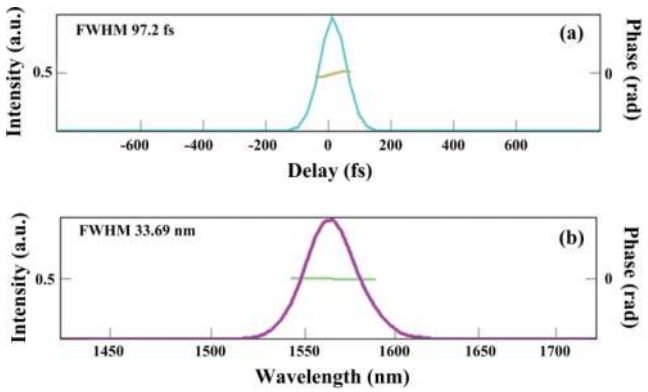

Figure 11. The measured pulse duration (a) and spectral width (b) of pulses from the nonlinear fiber amplifier.

Furthermore, a PPLN with 20.9-μm poling period and 0.3-mm length was used for frequency-doubling the amplified laser and checking the available peak power at 1560 nm. A pair of lens was used to focus and collimate the input and output beam on the PPLN, respectively. The output average power at 1560 nm and the corresponding SHG is shown in **Figure 12**. The highest SHG conversion efficiency was obtained as 56.3% with 302 mW incident power at 1560 nm. Further increasing the power at 1560 nm induced decay of conversion efficiency, shown as the black squares in **Figure 12**.

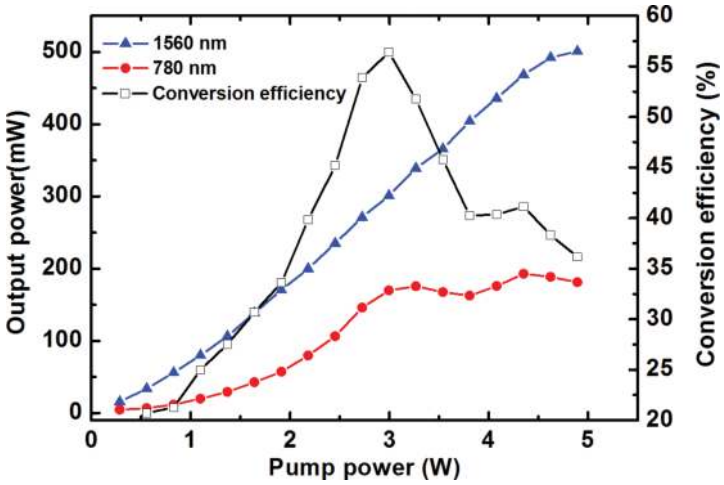

Figure 12. The output average power of 1560 nm (blue triangles) and 780 nm (red circles), and the SHG conversion efficiency.

To extract more energy from the double-pass amplifier, we will increase the number of the replicas from 8 to 16 and 32. The results for ×16 and ×32 replicas are still under investigation.

In conclusion, a divided fiber laser fiber amplifier delivering 500 mW average power at 1560 nm by the interplay between divided prechirped pulse amplification and nonlinear pulse compression. A small core double-clad erbium-doped fiber with anomalous dispersion carries out the pulse amplification and simultaneously compresses the laser pulses such that a separate compressor is no longer necessary. A numeric simulation reveals the existence of an optimum fiber length for producing a transform-limited pulse. Furthermore, frequency doubling to 780 nm with 170-mW average power is realized by using a PPLN at room temperature.

http://dx.doi.org/10.5772/64209

5. Repetition rate stabilization

Fiber-based frequency comb is recognized as the key breakthrough in the field of optics for it brings high accuracy in frequency domain as well as low jitter in time domain [49, 64–67]. Principally, as a frequency comb, two RF frequencies, f_{ceo} and f_{rep}, are required to be stabilized to external references. Therefore, the optical frequencies can be written as $\nu = m \times f_{rep} + f_{ceo}$, where m is a large integer of order 10^6 that indexes the comb line. Nevertheless, recent developments in adaptive dual-comb spectroscopy successfully employed free-running mode-locked lasers where the f_{ceo} instabilities could be compensated by data acquisition and electronic signal processing [68, 69]. Therefore, high accuracy f_{rep} stabilization of passively ML lasers is of great importance.

The relatively mature method for f_{rep} locking is to use a piezoelectric ceramic transducer (PZT) to control the geometrical length L of the laser cavity, and the best locking accuracy is in the range of ±0.5 mHz with the corresponding SD of 220 μHz [70]. However, the PZT-based stabilization encounters many limitations, such as significant positioning errors, hysteresis effect, bulky-design, and the need for time-consuming alignment.

In this section, we focus on the f_{rep} stabilization by using optical pumping scheme which can be achieved via resonantly enhanced optical nonlinearity or so-called pump-induced refractive index change (RIC) in doped fibers. In optical pumping scheme, the f_{rep} is stabilized by modulating the refractive index n, while keeping the geometrical cavity length L fixed. In the past, this method has been successfully applied in fiber switch where a low pump power and a short length doped fiber are sufficient for the switching [71]. Moreover, the validity of this concept has also been achieved in coherent combining and adaptive interferometry [72]. In 2013, Rieger et al. reported all-optical stabilized repetition rate by using the RIC-based method. With the help of thermos-electric element, over 12-h long-term stabilization was achieved in an NPE-mode-locked Er-doped fiber laser, while the SD of repetition rate drift was measured to be 22 mHz. A recent experiment extends this concept to Yb-fiber laser and achieves 1.39-mHz SD of residual fluctuation in an hour measurement [73].

As reported in Ref. [74], a commercial available pump current supply can provide a minimum resolution of pump power as 1.5 μW and thus achieve a controlling accuracy of 0.05 Hz, which is more than two orders of magnitude than PZT-based method. Therefore, an interesting experiment worth to do is to use RIC-method to achieve high-precision f_{rep} stabilization. So far, the RIC method has been fully investigated in NPR mode-locked lasers, which applied non-PM fibers and components [73–75], and the locking accuracy limited to ~mHz. Considering the environmental perturbation on non-PM fiber, a straightforward idea is to implement RIC method in a PM fiber laser. Therefore, the following part will discuss high-precision repetition rate stabilization by using RIC method in a PM figure-eight laser cavity.

The laser setup shown in **Figure 13** is same as **Figure 4(a)**, except the net dispersion of laser cavity. In the current experiment setup for all-optical repetition stabilization, a 56-cm-long Er^{3+}-doped fiber (EDF2) is spliced asymmetrically in the NALM to act as a frequency controller, while the LD3, which is controlled by the error signal from frequency mixer, provides the

feedback modulating pump power via WDM3 on EDF2. Besides, a segment of DCF38 is used to compensate the anomalous dispersion of PM1550 fiber. The dispersion of linear loop and the NALM was estimated numerically to be −0.208 and 0.025 ps^2, producing −0.183 ps^2 net dispersion for the whole cavity. Self-started mode-locking in multiple-pulse regime can be achieved by over-pumping method, and stable single-pulse operation can be obtained by decreasing the pump power of LD1 and LD2. At fundamental repetition rate of 11.9 MHz, the figure-eight laser cavity delivers 1.5-mW average power via CP2.

The repetition rate was detected by PD3 and successively compared with standard reference (Rb clock) in a frequency mixer to produce the error signal. Subsequently, the error signal was filtered and amplified by low-noise voltage preamplifier with frequency cutoff at 1 MHz and a maximum voltage gain of 5×10^4 and further processed by a proportional-integral-derivative (PID) controller.

The long-term stabilization was depicted in **Figure 14**. As low as 27-μHz accuracy is achieved within 16-h measurement. The inset of **Figure 14** magnifies the measured dates from 30,000 to 31,000 s and shows fluctuation range within ±0.1 mHz. Typically, thermal effect, Kerr nonlinear effect, pump-induced nonlinear effect, and random acoustic perturbations contribute to the precision of f_{rep} stabilization. For our experiment, a temperature-controlled incuba-

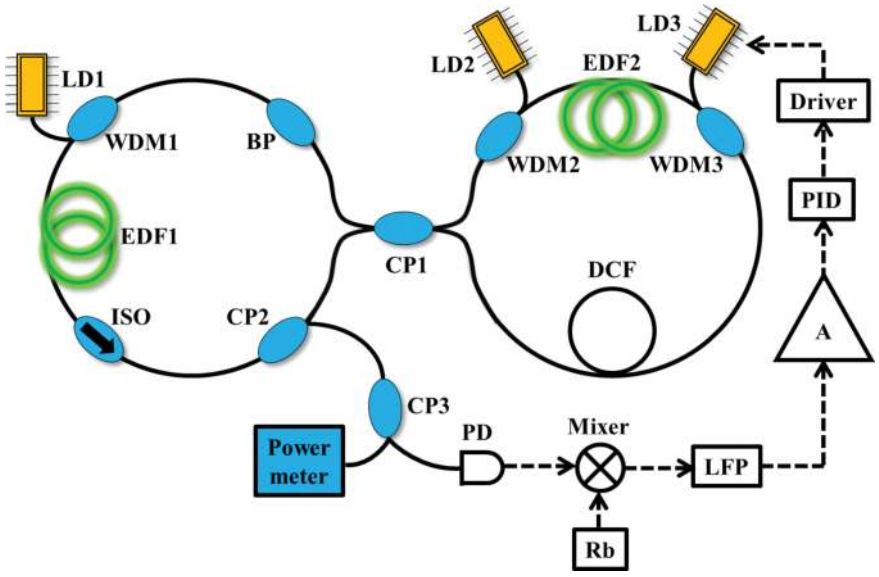

Figure 13. Experimental setup. LD1, LD2, and LD3: pump diodes at 976 nm; WDM1, WDM2, and WDM3: 980/1550 nm wavelength division multiplexers; EDF1, EDF2: erbium-doped fiber; BP: 2-nm bandpass filter centered at 1550 nm; CP1, CP2, and CP3: 1550 nm couplers with splitting ratio of 45:55, 30:70, and 50:50, respectively; DCF: dispersion compensation fiber; PD: photodiode detector; Rb: Rubidium clock; LFP: low-pass filter; A: electronic amplifier; PID: proportional–integral–derivative controller; Driver: precision current source.

http://dx.doi.org/10.5772/64209

tor with a ripple of 0.2°C was used to take the laser cavity to isolate environmental perturbation. As for Kerr-nonlinearity, the RIC is proportional to the traveling power of resonant laser. Assuming 5-mW traveling power in NALM, the Kerr-induced RIC is estimated as 1.2×10^{-7}/mW, having the same order of magnitude of the pump-induced RIC (2.1×10^{-7}/mW). However, when the pump power of LD3 increased from 30 to 205 mW, only 1.6% of output power change was observed, which means little change on the dynamic process of pulse evolution in NALM. Thus, the Kerr-induced RIC is near ~1% of the RIC by pump-induced nonlinearity. Therefore, we postulate that the nonlinearity on the RIC of fibers owes to pump-induced nonlinear effect and thermal effect rather than Kerr effect.

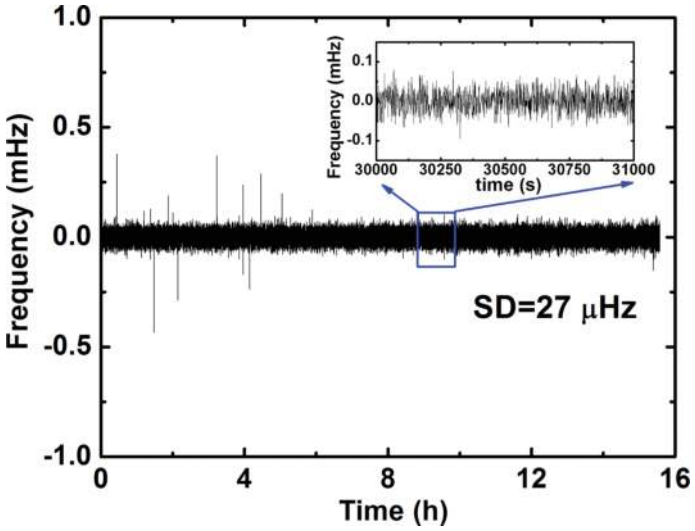

Figure 14. The long-time stabilization of repetition rate.

6. Conclusion

In this chapter, we first present several types of mode-locked fiber lasers, as well as their derivatives for SC generation. Second, an effective method named DPA was applied in Er-doped fiber laser system allowing simultaneous pulse amplification and compression so that additional pulse compressor is no longer needed. With ×8 replicas in DPA, as high as 500-mW average power was achieved and the highest SHG conversion efficiency was measured to be 56.3%. Third, an all-optical method, named as pump-induced nonlinearity, is applied to stabilize the repetition rate of a figure-eight Er-doped fiber laser, achieving as low as 27-μHz accuracy within 16-h measurement.

Author details

Qiang Hao, Tingting Liu and Heping Zeng*

*Address all correspondence to: hpzeng@phy.ecnu.edu.cn

Shanghai Key Laboratory of Modern Optical System, Engineering Research Center of Optical Instrument and System (Ministry of Education), School of Optical-Electrical and Computer Engineering, University of Shanghai for Science and Technology, Shanghai, China

References

[1] Hao, Q.; Li, W. & Zeng, H. (2007). Double-clad fiber amplifier for broadband tunable ytterbium-doped oxyorthosilicates lasers, *Opt. Express*, Vol. 15(25), 16754–16759.

[2] Xu, J.; Wu, S.; Liu, J.; Li, Y.; Ren, J.; Yang, Q. & Wang, P. (2014). All-polarization-maintaining femtosecond fiber lasers using graphene oxide saturable absorber, *IEEE Photon. Technol. Lett*., Vol. 26(4), 346–348.

[3] Albert, A.; Couderc, V.; Lefort, L. & Barthelemy, A. (2004). High-energy femtosecond pulses from an ytterbium-doped fiber laser with a new cavity design, *IEEE Photon. Technol. Lett*., Vol. 16(2), 416–418.

[4] Morin, F.; Druon, F.; Hanna, M. & Georges, P. (2009). Microjoule femtosecond fiber laser at 1.6 microm for corneal surgery applications, *Opt. Lett*., Vol. 34(13), 1991–1993.

[5] Kieu, K.; Mehravar, S.; Gowda, R.; Norwood, R. A. & Peyghambarian, N. (2013). Label-free multi-photon imaging using a compact femtosecond fiber laser mode-locked by carbon nanotube saturable absorber, *Biomed. Opt. Express*, Vol. 4(10), 2187.

[6] Li, W.; Hao, Q.; Yan, M. & Zeng, H. (2009). Tunable flat-top nanosecond fiber laser oscillator and 280 W average power nanosecond Yb-doped fiber amplifier, *Opt. Express*, Vol. 17(12), 10113–10118.

[7] Xu, C. & Wise, F. W. (2013). Recent advances in fiber lasers for nonlinear microscopy, *Nat. Photonics*, Vol. 7(11), 875–882.

[8] Shi, W.; Fang, Q.; Zhu, X.; Norwood, R. A. & Peyghambarian, N. (2014). Fiber lasers and their applications [Invited], *Appl. Opt*., Vol. 53(28), 6554–6568.

[9] Yang, K.; Li, W.; Yan, M.; Shen, X.; Zhao, J. & Zeng, H. (2012). High-power ultra-broadband frequency comb from ultraviolet to infrared by high-power fiber amplifiers, *Opt. Express*, Vol. 20(12), 12899–12905.

[10] Dudley, J. M. & Coen, S. (2002). Coherence properties of supercontinuum spectra generated in photonic crystal and tapered optical fibers, *Opt. Lett*., Vol. 27(13), 1180–1182.

[11] Wan, P.; Yang, L. & Liu, J. (2013). All fiber-based Yb-doped high energy, high power femtosecond fiber lasers, *Opt. Express*, Vol. 21(24), 29854.

[12] Nicholson, J. W. & Andrejco, M. (2006). A polarization maintaining, dispersion managed, femtosecond figure-eight fiber laser, *Opt. Express*, Vol. 14(18), 8160–8167.

[13] Baumgartl, M.; Ortaç, B.; Limpert, J. & Tünnermann, A. (2012). Impact of dispersion on pulse dynamics in chirped-pulse fiber lasers, *Appl. Phys. B*, Vol. 107(2), 263–274.

[14] Iii, I. N. (1991). All-fiber ring soliton laser mode locked with a nonlinear mirror, *Opt. Lett*., Vol. 16(8), 539–541.

[15] Tamura, K.; Ippen, E. P.; Haus, H. A. & Nelson, L. E. (1993). 77-fs pulse generation from a stretched-pulse mode-locked all-fiber ring laser, *Opt. Lett*., Vol. 18(13), 1080.

[16] Tamura, K.; Doerr, C. R.; Nelson, L. E.; Haus, H. A. & Ippen, E. P. (1994). Technique for obtaining high-energy ultrashort pulses from an additive-pulse mode-locked erbium-doped fiber ring laser, *Opt. Lett*., Vol. 19(1), 46–48.

[17] Herda, R. & Okhotnikov, O. G. (2004). Dispersion compensation-free fiber laser mode-locked and stabilized by high-contrast saturable absorber mirror, *IEEE J. Quantum Elect*., Vol. 40(7), 893–899.

[18] Runge, A. F. J.; Aguergaray, C.; Provo, R.; Erkintalo, M. & Broderick, N. G. R. (2014). All-normal dispersion fiber lasers mode-locked with a nonlinear amplifying loop mirror, *Opt. Fiber Technol*., Vol. 20(6), 657–665.

[19] Oktem, B.; Ulgudur, C. & Ilday, F. O. (2010). Soliton-similariton fibre laser, *Nat. Photon*., Vol. 4(5), 307–311.

[20] Abdelalim, M. A.; Logvin, Y.; Khalil, D. A. & Anis, H. (2009). Properties and stability limits of an optimized mode-locked Yb-doped femtosecond fiber laser, *Opt. Express*, Vol. 17(4), 2264–2279.

[21] Zhao, L. M.; Tang, D. Y.; Cheng, T. H.; Tam, H. Y. & Lu, C. (2007). Bound states of dispersion-managed solitons in a fiber laser at near zero dispersion, *Appl. Opt*., Vol. 46(21), 4768–4773.

[22] Chong, A.; Renninger, W. H. & Wise, F. W. (2007). All-normal-dispersion femtosecond fiber laser with pulse energy above 20 nJ, *Opt. Lett*., Vol. 32(16), 2408–2410.

[23] Erkintalo, M.; Aguergaray, C.; Runge, A. & Broderick, N. G. (2012). Environmentally stable all-PM all-fiber giant chirp oscillator, *Opt. Express*, Vol. 20(20), 22669–22674.

[24] Agrawal, G. P. (2001). *Applications of nonlinear fiber optics* (1st edn): Academic Press; 525 B Street, Suite 1900, San Diego, California 92101–4495, USA.

[25] Senoo, Y.; Nishizawa, N.; Sakakibara, Y.; Sumimura, K.; Itoga, E.; Kataura, H. & Itoh, K. (2010). Ultralow-repetition-rate, high-energy, polarization-maintaining, Er-doped, ultrashort-pulse fiber laser using single-wall-carbon-nanotube saturable absorber, *Opt. Express*, Vol. 18(20), 20673–20680.

[26] Hofer, M.; Fermann, M. E.; Galvanauskas, A.; Harter, D. & Windeler, R. S. (1998). High-power 100-fs pulse generation by frequency doubling of an erbium ytterbium-fiber master oscillator power amplifier, *Opt. Lett*., Vol. 23(23), 1840–1842.

[27] Takayanagi, J.; Kanamori, S.; Suizu, K.; Yamashita, M.; Ouchi, T.; Kasai, S.; Ohtake, H.; Uchida, H.; Nishizawa, N. & Kawase, K. (2008). Generation and detection of broadband coherent terahertz radiation using 17-fs ultrashort pulse fiber laser, *Opt. Express*, Vol. 16(17), 12859–12865.

[28] Gaponov, D. A.; Kotov, L. V.; Likhachev, M. E.; Bubnov, M. M.; Cabasse, A.; Oudar, J. L.; Fevrier, S.; Lipatov, D. S.; Vechkanov, N. N.; Guryanov, A. N. & Martel, G. (2012). High power all-fibered femtosecond master oscillator power amplifier at 1.56 μm, *Opt. Lett*., Vol. 37(15), 3186–3188.

[29] Tang, D. Y.; Zhao, L. M.; Zhao, B. & Liu, A. Q. (2005). Mechanism of multisoliton formation and soliton energy quantization in passively mode-locked fiber lasers, *Phys. Rev. A*, Vol. 72(4), 043816.

[30] Takayanagi, J.; Nishizawa, N.; Nagai, H.; Yoshida, M. & Goto, T. (2005). Generation of high-power femtosecond pulse and octave-spanning ultrabroad supercontinuum using all-fiber system, *IEEE Photonic. Technol. Lett*., Vol. 17(1), 37–39.

[31] Chen, Y.; Räikkönen, E.; Kaasalainen, S.; Suomalainen, J.; Hakala, T.; Hyyppä, J. & Chen, R. (2010). Two-channel hyperspectral LiDAR with a supercontinuum laser source, *Sensors*, Vol. 10(7), 7057–7066.

[32] Kaminski, C. F.; Watt, R. S.; Elder, A. D.; Frank, J. H. & Hult, J. (2008). Supercontinuum radiation for applications in chemical sensing and microscopy, *Appl. Phys. B*, Vol. 92(3), 367–378.

[33] Rulkov, A.; Vyatkin, M.; Popov, S.; Taylor, J. & Gapontsev, V. (2005). High brightness picosecond all-fiber generation in 525–1800 nm range with picosecond Yb pumping, *Opt. Express*, Vol. 13(2), 377–381.

[34] Hao, Q.; Guo, Z.; Liu, Y.; Li, W.; Zhang, Q. & Zeng, H. (2014). Spectrally tailored supercontinuum generation from single-mode-fiber amplifiers, *Appl. Phys. Lett*., Vol. 104(20), 201112.

[35] Tao, Z.; Yan, W.; Liu, L.; Li, L.; Oda, S.; Hoshida, T. & Rasmussen, J. C. (2011). Simple fiber model for determination of XPM effects, *J. Lightwave Technol*., Vol. 29(7), 974–986.

[36] Kudlinski, A.; Pureur, V.; Bouwmans, G. & Mussot, A. (2008). Experimental investigation of combined four-wave mixing and Raman effect in the normal dispersion regime of a photonic crystal fiber, *Opt. Lett*., Vol. 33(21), 2488–2490.

[37] Nodop, D.; Jauregui, C.; Schimpf, D.; Limpert, J. & Tünnermann, A. (2009). Efficient high-power generation of visible and mid-infrared light by degenerate four-wave-mixing in a large-mode-area photonic-crystal fiber, *Opt. Lett*., Vol. 34(22), 3499–3501.

[38] Hao, Q. & Huang, Y. C. (2013). Two-octave polarized supercontinuum generated from a Q-switched laser pumped doubly resonant parametric oscillator, *Opt. Lett*., Vol. 38(11), 1863–1865.

[39] Brown, W. J.; Kim, S. & Wax, A. (2014). Noise characterization of supercontinuum sources for low-coherence interferometry applications, *J. Opt. Soc. Am. A Opt. Image Sci. Vis*., Vol. 31(12), 2703–2710.

[40] Klose, A.; Ycas, G.; Maser, D. L. & Diddams, S. A. (2014). Tunable, stable source of femtosecond pulses near 2 μm via supercontinuum of an erbium mode-locked laser, *Opt. Express*, Vol. 22(23), 28400.

[41] Wadsworth, W.; Joly, N.; Knight, J.; Birks, T.; Biancalana, F. & Russell, P. (2004). Supercontinuum and four-wave mixing with Q-switched pulses in endlessly single-mode photonic crystal fibres, *Opt. Express*, Vol. 12(2), 299–309.

[42] Holdynski, Z.; Napierala, M.; Mergo, P. & Nasilowski, T. (2015). Experimental investigation of supercontinuum generation in photonic crystal fibers pumped with sub-ns pulses, *J. Lightwave Technol*., Vol. 33(10), 2106–2110.

[43] Cumberland, B. A.; Travers, J. C.; Popov, S. V. & Taylor, J. R. (2008). 29 W high power CW supercontinuum source, *Opt. Express*, Vol. 16(8), 5954–5962.

[44] Qiang, H. & Heping, Z. (2014). Cascaded four-wave mixing in nonlinear Yb-doped fiber amplifiers, *IEEE J. Sel. Top. Quant*., Vol. 20(5), 900205.

[45] Chen, K. K.; Alam, S.; Price, J. H. V.; Hayes, J. R.; Lin, D.; Malinowski, A.; Codemard, C.; Ghosh, D.; Pal, M.; Bhadra, S. K. & Richardson, D. J. (2010). Picosecond fiber MOPA pumped supercontinuum source with 39 W output power, *Opt. Express*, Vol. 18(6), 5426–5432.

[46] Kudlinski, A.; George, A. K.; Knight, J. C.; Travers, J. C.; Rulkov, A. B.; Popov, S. V. & Taylor, J. R. (2006). Zero-dispersion wavelength decreasing photonic crystal fibers for ultraviolet-extended supercontinuum generation, *Opt. Express*, Vol. 14(12), 5715–5722.

[47] Shen, X.; He, B.; Zhao, J.; Liu, Y.; Bai, D.; Yang, K.; Wang, C.; Liu, G.; Luo, D.; Liu, F.; Hao, Q.; Li, W. & Zeng, H. (2015). Repetition rate stabilization of an erbium-doped all-fiber laser via opto-mechanical control of the intracavity group velocity, *Appl. Phys. Lett*., Vol. 106(3), 31117.

[48] Xuling, S.; Wenxue, L.; Ming, Y. & Heping, Z. (2012). Electronic control of nonlinear-polarization-rotation mode locking in Yb-doped fiber lasers, *Opt. Lett*., Vol. 37(16), 3426–3428.

[49] Sinclair, L. C.; Coddington, I.; Swann, W. C.; Rieker, G. B.; Hati, A.; Iwakuni, K. & Newbury, N. R. (2014). Operation of an optically coherent frequency comb outside the metrology lab, *Opt. Express*, Vol. 22(6), 6996.

[50] Lee, C.; Chu, S. T.; Little, B. E.; Bland-Hawthorn, J. & Leon-Saval, S. (2012). Portable frequency combs for optical frequency metrology, *Opt. Express*, Vol. 20(15), 16671–16676.

[51] Reichel, S. & Zengerle, R. (1999). Effects of nonlinear dispersion in EDFA's on optical communication systems, *J. Lightwave Technol*., Vol. 17(7), 1152–1157.

[52] Mahran, O. & Aly, M. H. (2016). Performance characteristics of dual-pumped hybrid EDFA/Raman optical amplifier, *Appl. Opt*., Vol. 55(1), 22–26.

[53] Ju, H. L.; You, M. C.; Young, G. H.; Haeyang, C.; Sang, H. K. & Sang, B. L. (2005). A detailed experimental study on single-pump Raman/EDFA hybrid amplifiers: static, dynamic, and system performance comparison, *J. Lightwave Technol*., Vol. 23(11), 3484–3493.

[54] Varallyay, Z. & Jasapara, J. C. (2009). Comparison of amplification in large area fibers using cladding-pump and fundamental-mode core-pump schemes, *Opt. Express*, Vol. 17(20), 17242–17252.

[55] Eidam, T.; Hanf, S.; Seise, E.; Andersen, T. V.; Gabler, T.; Wirth, C.; Schreiber, T.; Limpert, J. & Tünnermann, A. (2010). Femtosecond fiber CPA system emitting 830 W average output power, *Opt. Lett*., Vol. 35(2), 94–96.

[56] Galvanauskas, A.; Cho, G. C.; Hariharan, A.; Fermann, M. E. & Harter, D. (2001). Generation of high-energy femtosecond pulses in multimode-core Yb-fiber chirped-pulse amplification systems, *Opt. Lett*., Vol. 26(12), 935–937.

[57] Ancona, A.; Roser, F.; Rademaker, K.; Limpert, J.; Nolte, S. & Tünnermann, A. (2008). High speed laser drilling of metals using a high repetition rate, high average power ultrafast fiber CPA system, *Opt. Express*, Vol. 16(12), 8958–8968.

[58] Kuznetsova, L. & Wise, F. W. (2007). Scaling of femtosecond Yb-doped fiber amplifiers to tens of microjoule pulse energy via nonlinear chirped pulse amplification, *Opt. Lett*., Vol. 32(18), 2671–2673.

[59] Sobon, G.; Kaczmarek, P.; Gluszek, A.; Sotor, J. & Abramski, K. M. (2015). μJ-level, kHz-repetition rate femtosecond fiber-CPA system at 1555 nm, *Opt. Commun*., Vol. 347, 8–12.

[60] Guichard, F.; Hanna, M.; Zaouter, Y.; Papadopoulos, D. N.; Druon, F. & Georges, P. (2014). Analysis of limitations in divided-pulse nonlinear compression and amplification, *IEEE J. Sel. Top. Quant*., Vol. 20(5), 619–623.

[61] Kong, L. J.; Zhao, L. M.; Lefrancois, S.; Ouzounov, D. G.; Yang, C. X. & Wise, F. W. (2012). Generation of megawatt peak power picosecond pulses from a divided-pulse fiber amplifier, *Opt. Lett*., Vol. 37(2), 253–255.

[62] Hao, Q.; Zhang, Q.; Sun, T.; Chen, J.; Guo, Z.; Wang, Y.; Guo, Z.; Yang, K. & Zeng, H. (2015). Divided-pulse nonlinear amplification and simultaneous compression, *Appl. Phys. Lett*., Vol. 106(10), 101103.

[63] Kienel, M.; Klenke, A.; Eidam, T.; Baumgartl, M.; Jauregui, C.; Limpert, J. & Tünnermann, A. (2013). Analysis of passively combined divided-pulse amplification as an energy-scaling concept, *Opt. Express*, Vol. 21(23), 29031.

[64] Cingoz, A.; Yost, D. C.; Allison, T. K.; Ruehl, A.; Fermann, M. E.; Hartl, I. & Ye, J. (2012). Direct frequency comb spectroscopy in the extreme ultraviolet, *Nature*, Vol. 482(7383), 68–71.

[65] Hsieh, Y. D.; Iyonaga, Y.; Sakaguchi, Y.; Yokoyama, S.; Inaba, H.; Minoshima, K.; Hindle, F.; Araki, T. & Yasui, T. (2014). Spectrally interleaved, comb-mode-resolved spectroscopy using swept dual terahertz combs, *Sci. Rep*., Vol. 4, 3816.

[66] Heinecke, D. C.; Bartels, A. & Diddams, S. A. (2011). Offset frequency dynamics and phase noise properties of a self-referenced 10 GHz Ti:sapphire frequency comb, *Opt. Express*, Vol. 19(19), 18440–18451.

[67] Locke, C. R.; Ivanov, E. N.; Light, P. S.; Benabid, F. & Luiten, A. N. (2009). Frequency stabilisation of a fibre-laser comb using a novel microstructured fibre, *Opt. Express*, Vol. 17(7), 5897–5904.

[68] Ideguchi, T.; Poisson, A.; Guelachvili, G.; Picque, N. & Hansch, T. W. (2014). Adaptive real-time dual-comb spectroscopy, *Nat. Commun*., Vol. 5, 3375.

[69] Schliesser, A.; Picqué, N. & Hänsch, T. W. (2012). Mid-infrared frequency combs, *Nat. Photon*., Vol. 6(7), 440–449.

[70] Zhang, W.; Han, H.; Zhao, Y.; Du, Q. & Wei, Z. (2009). A 350 MHz Ti:sapphire laser comb based on monolithic scheme and absolute frequency measurement of 729 nm laser, *Opt. Express*, Vol. 17(8), 6059–6067.

[71] Pantell, R. H.; Sadowski, R. W.; Digonnet, M. J. & Shaw, H. J. (1992). Laser-diode-pumped nonlinear switch in erbium-doped fiber, *Opt. Lett*., Vol. 17(14), 1026–1028.

[72] Fotiadi, A. A.; Zakharov, N.; Antipov, O. L. & Megret, P. (2009). All-fiber coherent combining of Er-doped amplifiers through refractive index control in Yb-doped fibers, *Opt. Lett*., Vol. 34(22), 3574–3576.

[73] Yang, K.; Hao, Q. & Zeng, H. (2015). All-optical high-precision repetition rate locking of an Yb-doped fiber laser, *IEEE Photon. Technol. Lett*., Vol. 27(8), 852–855.

[74] Bo, N.; Dong, H.; Peng, D. & Jianye, Z. (2013). Long-term repetition frequency stabilization of passively mode-locked fiber lasers using high-frequency harmonic synchronization, *IEEE J. Quantum Electron.*, Vol. 49(6), 503–510.

[75] Rieger, S.; Hellwig, T.; Walbaum, T. & Fallnich, C. (2013). Optical repetition rate stabilization of a mode-locked all-fiber laser, *Opt. Express*, Vol. 21(4), 4889–4895.